Journal of Constructional Steel Research 66 (2010) 1354–1365

Contents lists available at ScienceDirect

Journal of Constructional Steel Research

journal homepage: www.elsevier.com/locate/jcsr

Tests and analyses of a full-scale post-tensioned RCS frame subassembly

Chung-Che Chou [a,b,*], Jun-Hen Chen [c]

[a] Department of Civil Engineering, National Taiwan University, Taipei, Taiwan
[b] National Center for Research on Earthquake Engineering, Taipei, Taiwan
[c] Department of Civil Engineering, National Chiao Tung University, Hsinchu, Taiwan

ARTICLE INFO

Article history:
Received 16 November 2009
Accepted 26 April 2010

Keywords:
Post-tensioned self-centering frame
Cyclic test
Analytical model
Time-history analysis

ABSTRACT

A series of cyclic tests of a full-scale one-story two-bay specimen frame, a substructure of a three-story post-tensioned (PT) self-centering (SC) building using reinforced concrete columns and steel beams, were conducted in the Taiwan National Center for Research on Earthquake Engineering. The objectives of the tests were: (1) to examine the connection performance, progress of damage, and strength degradation of the frame, (2) to assess the hysteretic responses of the frame subjected to various loading patterns, and (3) to study the effects of column restraints on the frame expansion. Time-history analyses of the three-story PT building subjected to the design basis earthquake (DBE) and the maximum considered earthquake (MCE) were conducted to investigate seismic demands of the proposed system. These tests confirmed the SC response of the PT frame and explored failure of the beam compression toe, which was never observed in prior tests of beam–column subassemblages. The nonlinear structural analysis computer program PISA could be used to simulate the experimental results well; time-history analyses of the three-story building showed that the proposed frame can meet seismic demands by MCE level ground motions.

1. Introduction

In the past few decades, mixed steel–concrete structural frames have gained popularity in the construction of buildings. These frames are named as RCS (reinforced concrete steel) systems with steel beams and reinforced concrete columns. In the US and Japan, RCS frames have been developed as an alternative to typical reinforced concrete construction for buildings because of (1) reductions in concrete form work, (2) increased space availability by enlarging beam spans, and (3) economics in construction by using precast subassemblies [1–3]. Special consideration is given to detail RCS connections where the steel beam runs continuous through the concrete column to form an integral component (Fig. 1(a)). The light steel column embedded inside the concrete column is used for erection loads only, and the RCS connection, which is distinct from the more typical SRC (steel reinforced concrete) connection [4,5], is designed to transfer large forces between the steel beam and the concrete column. Test data confirmed that the cyclic performance of well-designed RCS connections can achieve high levels of interstory drift (i.e. 4%). The maximum strength is controlled by either (1) local buckling of the beam flanges and web that occur after significant yielding in the hinge region outside the column face, or (2) shear yielding of the steel web panel and compression failure of concrete in the connection. Significant strength reduction and residual deformation are typical behaviors at the end of connection tests.

The connection configuration in this study is shown in Fig. 1(b), where the post-tensioning strands are utilized to compress the steel beams against the concrete column. A reduced flange plate (RFP), which was proposed by Chou and co-workers [6–9], is incorporated in the connection to increase energy dissipation. The size of the RFP is determined based on expected moment of the RFP at a target drift, where a maximum tensile strain in the narrowest section is limited to 0.1 [9]. Slotted holes near the column face are used to allow for pass of bolts for connecting the T-shaped stiffener and the beam flange and have no adverse effects on the energy dissipation based on the prior studies [7,9]. This detail eliminates the embedment of a steel beam in the connection, improving the constructability of traditional RCS connections in the field. The post-tensioned (PT) connection also decreases residual deformations by the elastic responses of PT strands and steel beams. Many researchers have experimentally validated the self-centering (SC) behaviors of PT connections with gap-opening, closing at the beam-to-column interface [7–12]. Ricles et al. [10,11] utilized PT strands as the SC element and angles as the energy-dissipating element to eliminate field welding and reduce residual deformations of steel moment connections. Cyclic

* Corresponding author at: Department of Civil Engineering, National Taiwan University, Taipei, Taiwan. Tel.: +886 2 3366 4349; fax: +886 2 2739 6752.
E-mail address: cechou@ntu.edu.tw (C.-C. Chou).

0143-974X/$ – see front matter © 2010 Elsevier Ltd. All rights reserved.
doi:10.1016/j.jcsr.2010.04.013

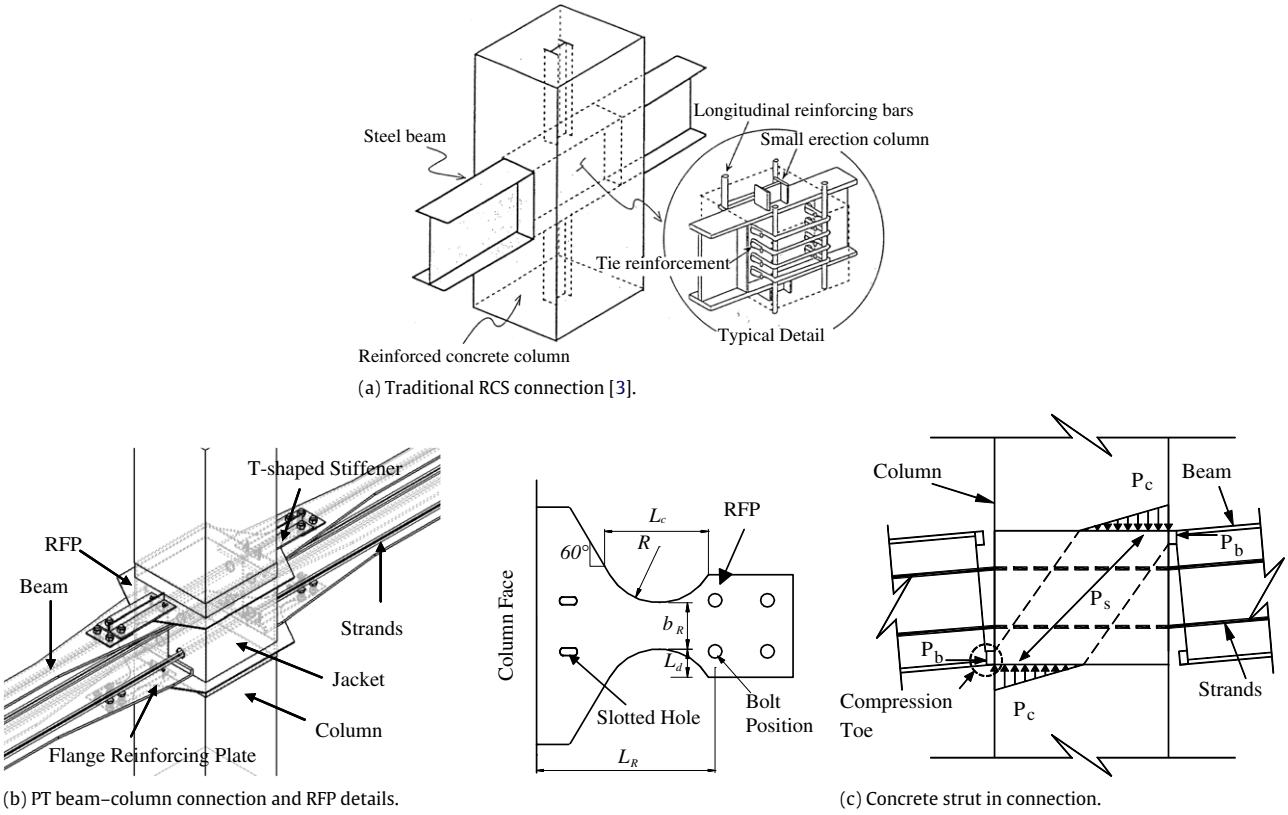

(a) Traditional RCS connection [3].

(b) PT beam–column connection and RFP details.

(c) Concrete strut in connection.

Fig. 1. Beam–column connection details.

tests demonstrated SC hysteretic responses of the PT connection, and frame dynamic analyses showed superior seismic performance in PT frames than in moment-resisting frames (MRFs) with typical welded connections. Christopoulos et al. [12] tested a PT connection with energy-dissipating bars, successfully eliminating permanent damage of energy-dissipating devices after cyclic loads. A flag-shaped hysteretic response of the PT connection could be simulated analytically by using rotational springs in the beam–column joint.

When the gap opens at the beam-to-column interface, the concrete slab if it does not open along the column lines produces restraints to PT connections, altering the SC capability [13]. Garlock et al. [14–16] suggested the collector beams or bays to transfer floor inertia forces to the PT frame and accommodate frame expansion. Kim and Christopoulos [17] proposed details along the boundaries of the slabs that allow for the gap-openings to be accommodated and elimination of the restraints to PT connections. Recently, Chou et al. [9] demonstrated that the PT connection with a continuous composite slab self-centers with low residual deformations as long as negative connection moments provided by slab reinforcements are considered in design. Chou et al. [18] also showed similar cyclic responses between a bare PT connection and a composite PT connection with a discontinuous composite slab, which opens freely along with the gap-opening at the beam-to-column interface.

The approach in seismic design, developed under the US PRESSS program coordinated by the University of California, San Diego [19,20] for precast concrete buildings with SC connections, was verified from a 3/5 scale five-story self-centering concrete test building. The SC behavior of the test building was extremely satisfactory without significant strength loss up to drift levels of 4.5%. This post-tensioning technology was successfully extended to steel MRFs by shake table tests of a 1/3 scale one-story two-bay frame [21]. A recent project focusing on the design and experimental performance of a steel SC-MRF was conducted at the Lehigh University [22]. The test structure for the experimental program was a 3/5 scale four-story two-bay SC-MRF. The static and pseudo-dynamic tests of this SC-MRF showed the self-centering capability of the frame and good energy dissipation of the web-friction device as observed in the connection test [23]. Sake table tests with a 1/3 scale steel MRF and SC-MRF also demonstrated that the maximum interstory drifts of the SC-MRF specimen are similar or slightly higher compared to those in the MRF specimen [24]. Tests conducted on large- or full-scale post-tensioned self-centering frames were rather limited. Thus, to understand system performance, a full-scale one-story two-bay PT frame (Fig. 2) was designed, built, and tested at the National Center for Research on Earthquake Engineering (NCREE), Taiwan. The three-story prototype building was designed for a high seismic location in either Taiwan or the US. The bay width was 5 m and the first-story height was 3.92 m. Several quasi-static load tests were conducted to cyclically load the frame to large drifts to examine the performance of the frame. This paper describes the detailed experimental observation, including damage of the beam and the RFP that occurred during the tests, and discusses an analytical computer model made after the tests for the correlation study. Inelastic time-history analyses of the prototype building subjected to 15 ground motions are conducted to examine seismic demands of the proposed frame at the design basis earthquake (DBE) and the maximum considered earthquake (MCE) levels.

2. Test program

2.1. Design of a prototype building

A procedure proposed by Garlock [14] was adopted to design a three-story PT prototype frame, which is required to self-center at the DBE and MCE earthquake levels. Fig. 2 shows the plan and

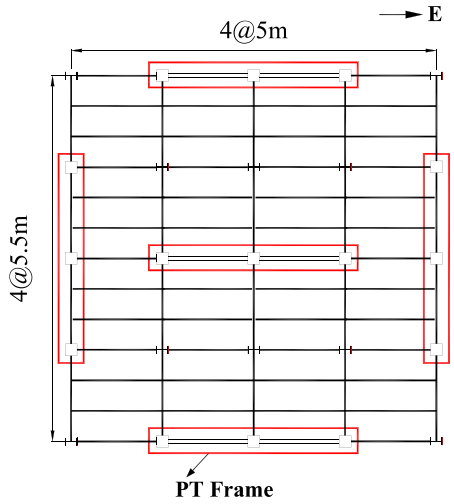

(a) Plan.

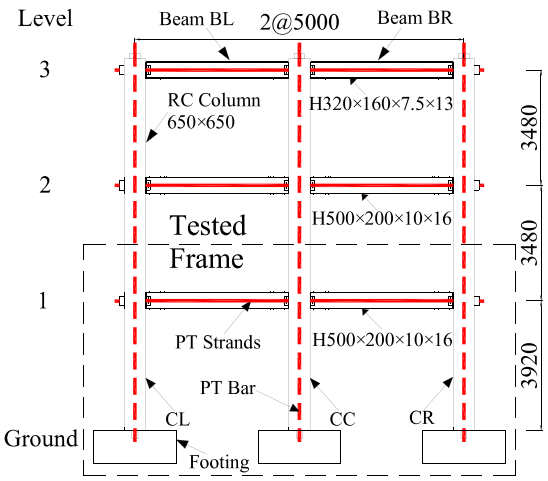

(b) Elevation.

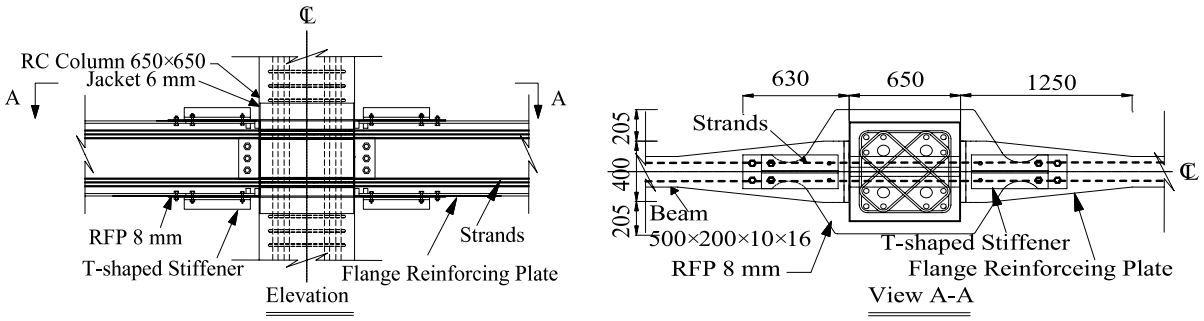

(c) PT Connection details.

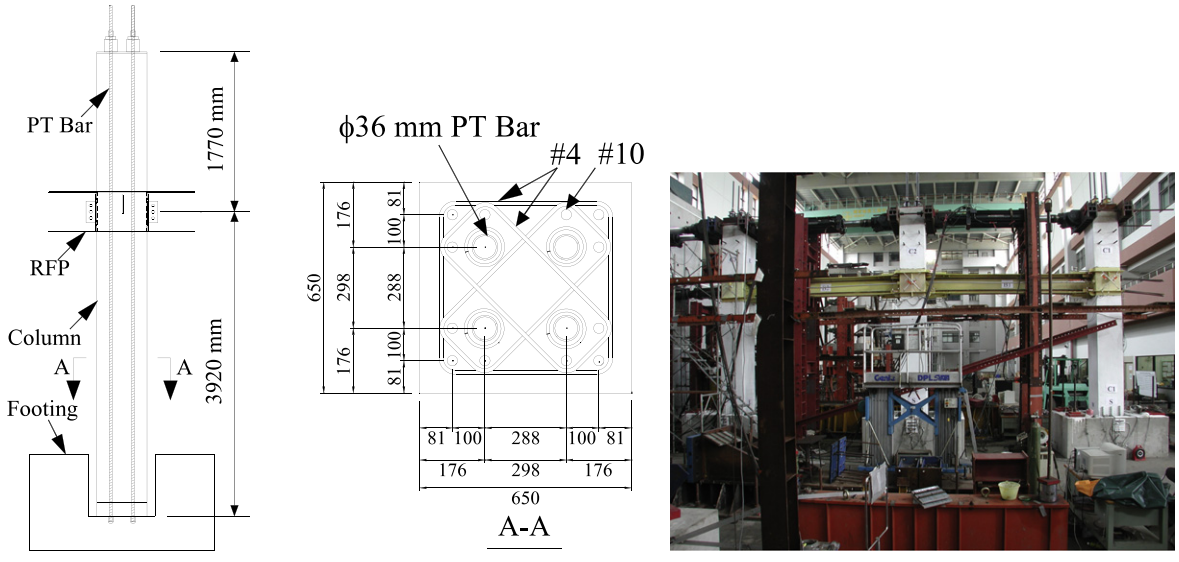

(d) PT column.

(e) Specimen frame.

Fig. 2. Three-story prototype building and specimen frame.

elevation of the prototype building, which was assumed to be located on stiff soil in Los Angeles, California. Three two-bay PT frames providing lateral load resistance in the east–west direction were considered in this study; each PT frame was composed of three PT reinforced concrete columns and six PT steel beams (Fig. 2(b)). Instead of using transverse reinforcement, a steel jacket was used to confine the concrete in the connection (Fig. 2(c)). The RFPs were shop-welded along the perimeter of the jacket and field-bolted to the beam flange following application of the post-tensioning force in the beam. A T-shaped stiffener was bolted outside the RFP to prevent the RFP from buckling in compression. No energy dissipation device was used at the base of PT columns so the bilinear elastic response was expected as seen in the prior studies [25,26].

The design dead loads were 5.28 kPa (110 psf) and 4.32 kPa (90 psf) for the floors and the roof while the live loads for the floors

Table 1
Prototype frame.

(a) Dimension and moment demands

Floor	Size	PT element number & size	A_{ST} (mm^2)	T_{in} (kN)	t_R (mm)	b_R (mm)	L_c (mm)	L_R (mm)	R	$\frac{M_E}{M_{np}}$	$\frac{M_D}{M_{np}}$	$\frac{M_L}{M_{np}}$	$\frac{M_{dem}}{M_{np}}$
3rd	H320 × 160 × 7.5 × 13	12–13 mm	1184	500	4	120	164	380	127	0.22	0.15	0.09	0.48
2nd	H500 × 200 × 10 × 16	12–13 mm	1184	900	8	120	246	450	127	0.29	0.05	0.03	0.37
1st	H500 × 200 × 10 × 16	12–15 mm	1579	900	8	120	246	450	127	0.34	0.05	0.03	0.42
Column	RC 650 × 650	4–36 mm	4072	1100	–	–	–	–	–	0.24	–	–	0.24

(b) Response in the reinforced beam at column face

Floor	Decompression			Yield	4% Drift			No column restraint		Column restraint	
	$\frac{M_{d,ST}}{M_{np}}$	$\frac{M_{d,R}}{M_{np}}$	$\frac{M_d}{M_{np}}$	$\frac{M_y}{M_{np}}$	$\frac{M_{ST}}{M_{np}}$	$\frac{M_R}{M_{np}}$	$\frac{M^a_{4\%}}{M_{np}}$	$\frac{P^b_{4\%}}{\phi_b P^c_{ry}}$	$\frac{P_{4\%}}{\phi_b P_{ry}} + \frac{M_{4\%}}{\phi_b M^d_{ry}}$	$\frac{\tilde{P}^e_{4\%}}{\phi_b P_{ry}}$	$\frac{\tilde{P}_{4\%}}{\phi_b P_{ry}} + \frac{\tilde{M}^f_{4\%}}{\phi^g_b M_{ry}}$
3rd	0.30	0.070	0.37	0.48	0.65	0.29	0.94	0.21	0.82	0.20	0.8
2nd	0.28	0.072	0.35	0.46	0.56	0.30	0.86	0.25	0.71	0.23	0.69
1st	0.28	0.072	0.35	0.46	0.64	0.29	0.93	0.29	0.80	0.34	0.88
Column	0.2	–	0.2	0.3	–	–	–	–	–	–	-

a = moment demand at 4% drift (no column restraint)
b = axial load at 4% drift (no column restraint)
c = Axial strength of the beam plus flange reinforcing plate
d = Yield moment of the beam plus flange reinforcing plate,
e = Axial load at a 4% drift (with column restraint)
f = moment demand at a 4% drift (with column restraint); $g = 0.9$

(c) Response in the unreinforced beam at the end of flange reinforcing plates

Floor	No column restraint			Column restraint		
	$\frac{P_{4\%}}{\phi_b P^a_{by}}$	$\frac{M_u}{\phi_b M^b_{by}}$	$\frac{P_{4\%}}{\phi_b P_{by}} + \frac{M^c_u}{\phi_b M_{by}}$	$\frac{\tilde{P}_{4\%}}{\phi_b P_{by}}$	$\frac{\tilde{M}^d_u}{\phi_b M_{by}}$	$\frac{\tilde{P}_{4\%}}{\phi_b P_{by}} + \frac{\tilde{M}_u}{\phi_b M_{by}}$
3rd	0.34	0.66	1.0	0.33	0.66	0.99
2nd	0.41	0.49	0.9	0.39	0.49	0.88
1st	0.46	0.54	1.0	0.51	0.57	1.08

a = Axial strength of the beam
b = Yield moment of the beam
c = Moment demand at the end of flange reinforcing plates (no column restraint)
d = Moment demand at the end of flange reinforcing plates (with column restraint)

and the roof were 2.39 kPa (50 psf). The same live load for the floors and the roof was used based on Taiwanese design practice. Effective seismic weights for the floors and the roof were 2320 kN and 1896 kN, respectively, resulting in a total seismic weight of the building equal to 6536 kN. The design followed IBC 2000 [27] with a force reduction factor R of 8, an overstrength Ω_0 of 3 and a deflection amplification factor C_d of 5.5. The mapped MCE spectral response acceleration at a short period S_S and one second S_1 was 1.5 g and 0.6 g, respectively. For the building located at site class D, the site coefficients F_a and F_v were 1.0 and 1.5, respectively, leading to design spectral response accelerations at a short period and one second of 1.0 g and 0.6 g, respectively. The structural period T and the seismic response coefficient C_s calculated by the codified method were 0.6 s and 0.125, respectively, so the seismic design base shear V_{des} for one PT frame was 272 kN. The selected beam and column sizes, RFP thickness t_R and narrowest width b_R, strand and PT bar areas A_{ST}, and initial PT force T_{in} are given in Table 1(a). The 650 × 650 mm reinforced concrete (RC) column contained 12–#10 longitudinal reinforcing bars, which were stopped near the column base-to-footing interface (Fig. 2(d)). The fixity of the column base was provided by four 36 mm diameter high strength PT bars, which were positioned at the center location, passing through the column base-to-footing interface, and anchored inside the footing. High strength Dywidag (DSI) bar was specified to the PT bar, and ASTM A 706M steel was specified for the transverse and longitudinal reinforcement. The specified 28-day concrete strength, f'_{cn}, was 28 MPa. A572 Grade 345 (50) steel was used for the steel beams, and ASTM A416 Grade 270 strands were passed along the beam webs and anchored outside the exterior columns (Fig. 2(b)). Moment demands at the beam-to-column interface and the column base due to seismic design load (M_E), dead load (M_D) and live load (M_L) are also given in Table 1(a). The code-based design moment in combination of these loading sources was M_{dem}, less than $0.55M_{np}$, where M_{np} was the beam nominal plastic moment capacity (neglecting the flange reinforcing plate contribution). M_{dem} less than $0.55M_{np}$ was used to determine the size of the beam based on the work by Garlock [14].

The PT connection behaves as a fully restrained moment connection provided the beam moment is less than the decompression moment, M_d, at the beam-to-column interface:

$$M_d = M_{d,ST} + M_{d,R} = \left[T_{in}\left(\frac{d_b}{2} - t_f\right)\right] + \left[T_R\left(d_b + t_R\right)\right] \quad (1)$$

where $M_{d,ST}$ and $M_{d,R}$ are the moments provided by the initial strand force, T_{in}, and the RFPs, respectively; T_R is the tensile force (smaller than the yield force by changing the length of the RFP) in the RFP at the onset of gap-opening at the beam-to-column interface (Fig. 3(a)); t_R is the thickness of the RFP; t_f is the thickness of the beam flange, and d_b is the beam depth. Prior to decompression, the post-tensioning forces, $T_{u,in}$ and $T_{l,in}$, in the strands do not change noticeably from the initial value, T_{in}; the tensile force, T_R, in the RFP is determined based on the axial deformation, Δ_{in}:

$$\Delta_{in} = \int_0^{L_R} \frac{4T_{in}}{E_s \times A}\mathrm{d}x \quad (2)$$

where A is the cross-sectional area of the beam plus flange reinforcing plates; E_s is the modulus of steel, and L_R is the length of the RFP (Fig. 1(b)).

The decompression moment was larger than the moments due to dead load and live load and was slightly smaller than the moment demand M_{dem} [14]. It was understood that significant inelastic stiffness occurs at the onset of RFP yielding not gap-opening at the beam-to-column interface. The connection moment

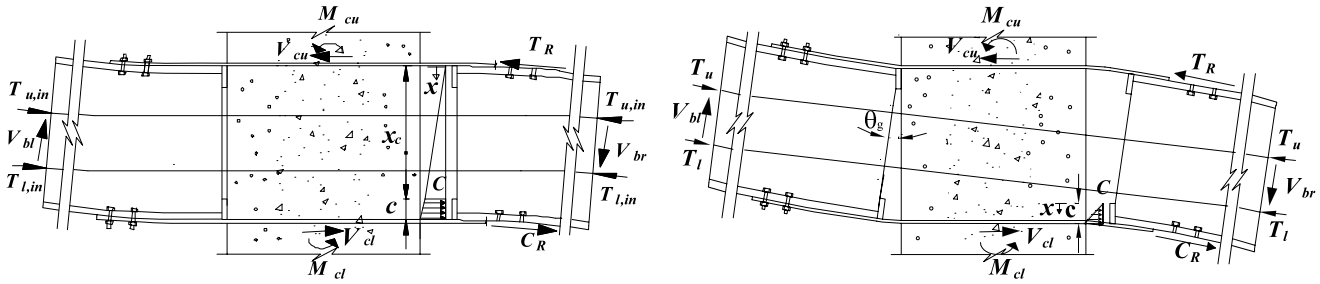

(a) Onset of gap-opening.

(b) Gap-opening rotation θ_g.

Fig. 3. Kinematics of the connection.

at the onset of RFP yielding was M_y, which included moments provided by the initial post-tensioning force in strands and yield forces in RFPs. The connection moment M_y was larger than $\alpha_y M_{dem}$, where $\alpha_y \geq 1.0$, indicating the elasticity of the PT frame under the code-based seismic load.

Since the RFPs provide energy dissipation in the PT connection as well as angles, friction plates, or bars among other studies, the relative rotation between the beam and column for specified hazard levels can be referred to the works by Rojas [28] or Kim and Christopoulos [17]. Under DBE and MCE ground motions, the interstory drifts of the frame ranged up to 3%–4.5%, respectively. Following the connection design procedure proposed by Chou et al. [9], the connection moment at a drift of 4%, $M_{4\%}$, was expected to be about $0.9M_{np}$ at the column face, $M_R \approx 0.3M_{np}$ of which was provided by the RFPs and $M_{ST} \approx 0.6M_{np}$ of which was provided by the strands (Table 1(b)):

$$M_{4\%} = M_{ST} + M_R = \left[T_{ST}\left(\frac{d_b}{2} - t_f\right)\right] + \left[T_R\left(d_b + \frac{t_R}{2} - t_f\right) + C_R\left(\frac{t_R}{2} + t_f\right)\right] \quad (3)$$

where T_{ST} is the strand force, and T_R and C_R are the tensile and compressive forces in the RFPs, respectively. These forces were estimated based on the gap-opening rotation θ_g (≈0.03 rad.) at the beam-to-column interface (Fig. 3(b)). Assuming that the shear strength of the jacket plate resisted forces in the RFPs, the thickness of the plate, *tj*, was calculated as

$$t_j = \frac{T_R + C_R}{2\phi 0.6F_{yj}\left(\frac{5}{6}d_c\right)} \quad (4)$$

where *Fyj* is the specified yield strength of the jacket plate; *dc* is the column width, and ϕ (=0.75) is the strength reduction factor. A factor of 5/6 is included to consider a parabolic shear stress distribution across the width of the jacket plate [1,5]. The joint shear strength was calculated based on the concrete strut, which is mobilized by beam compression toes. The strut, shown in Fig. 1(c), is similar to that used to model shear in RCS connections [3]. At an interstory drift of 4%, the compression stress of the concrete in a strut was 15 MPa, less than the allowable strength of $0.85f'_{cn}$ (=29 MPa) according to ACI 318 [29].

The values calculated by the moment–axial compression interaction equation at the column face and the beam section where the flange reinforcing plates are terminated are listed in Table 1(b) and (c), indicating that the steel beam remains elastic up to a 4% drift without considering column restraints. Considering the column restraints in the beam, the values show that the column restraint is significant on the first floor, increasing the value of axial load–bending moment interaction, and is minor on the upper floors. The analytical procedure for determining the effects of column restraints in the PT frame can be found elsewhere [30].

2.2. Construction of the specimen frame

Three concrete columns and three footings were fabricated in the precast yard and delivered to the laboratory. The footing with an embedded anchorage was first positioned in the laboratory (Fig. 4(a)) before erecting a column. The column was then aligned and temporarily post-tensioned to the footing (Fig. 4(b)). The steel beam was bolted to the shear tab of the jacket (Fig. 4(c)). Strands were placed along each side of the steel beam web, passed through the center column and anchored outside the exterior columns (Fig. 4(d)). Top and bottom RFPs were bolted to the beam flanges after application of PT forces in the beams. Finally, the PT bars in columns were stressed to meet the design force level (Table 1(a)). Each column stopped at the mid-height of the second story, at which two 1000 kN actuators (Act 1 and Act 2) were positioned between the reaction wall and the frame and one 1000 kN actuator (Act3 or Act 4) was positioned in each beam span (Fig. 5).

2.3. Test loading

The objectives of the test were to (1) examine the interaction between the damage of connections and the global damage sustained by the structure frame; (2) assess the hysteretic behavior of the frame subjected to various loading patterns, (3) observe the effects of column restraining on the frame elongation and the post-tensioning force in the beam, and (4) calibrate the analytical model of the specimen frame by using a rotational spring scheme for PT connections. Therefore, the cyclic loading protocol for steel connection tests [31] was adopted in this test program, and the specimen frame was tested until reaching the limitation of actuators to drift levels of 4%, slightly lower than 4.5% obtained from the PRESSS building test [20]. Asymmetric loading, which is not required by AISC [31] for connection tests, was not included in the test program. Based on the prior works by Kim and Christopoulos [17] and Chou et al. [9,18], if the slab can be separated along the column line, the effects of the slab on the gap-opening is minimal. Connection moments of the beam under either positive or negative bending are similar. This PT building adopted these slab details, so the slab (or diaphragm) was not included in the specimen frame. Loading from the column instead of the slab to the specimen was adopted to study the frame response and column restraints to the frame expansion. Although this method of loading did not represent what would actually occur in a real building with the separated slab system, it was also commonly used in other PT frame tests [22].

Center column (CC) displacement at the loading point was controlled as a target displacement; the interstory drift was defined as the horizontal displacement at this loading point divided by the column height of 5.66 m. The displacement history consisted of three cycles of interstory drift with amplitudes of 0.25%, 0.375%, 0.5%, 0.75%, and 1%, followed by two cycles of drift with amplitudes of 1.5%, 2%, 3%, and 4%. Two loading schemes were

(a) Footing alignment.

(b) Column erection.

(c) Beam installation.

(d) PT beam to column.

Fig. 4. Specimen frame assembly in the laboratory.

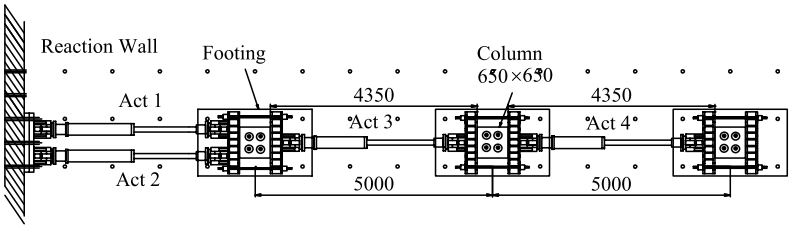

(a) Top view.

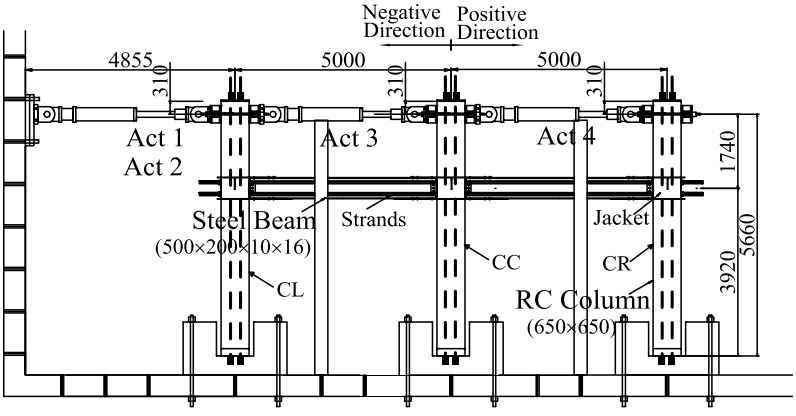

(b) Elevation.

Fig. 5. Specimen frame (unit: mm).

adopted in the test program. In the first loading scheme, the forces in Act 3 and Act 4 were slaved to three-quarter and one-quarter, respectively, the total forces in Act 1 and Act 2. Therefore, the shear force applied to columns CL and CR was half that applied to column CC at the loading point. Since the exterior column tops could expand with respect to center column CC, column restraint to the beam was minimal. This loading scheme was carried out for the first three tests, in which RFPs used to increase connection energy were only included in the first two tests. For the second loading scheme, relative lateral deformation between column tops

(a) Bending of beam flange (1st test). (b) Vertical stiffener (1st test). (c) Out-of-plane deformation of jacket (1st test).

(d) RFP fracture (1st test). (e) Beam-to-column gap-opening (3rd test). (f) Beam yielding (after 4th test).

Fig. 6. Observed performance in PT frame tests.

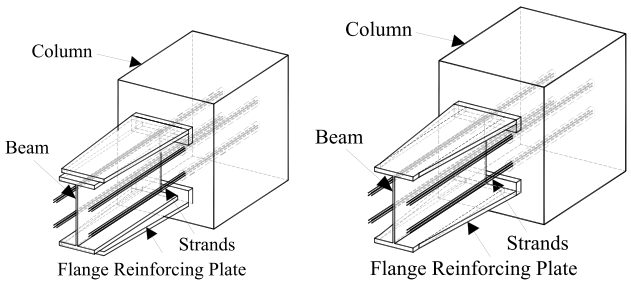

(a) Connection specimen. (b) Frame specimen.

Fig. 7. Flange reinforcing plate details.

was excluded to simulate the pin-supported boundary condition, producing full restraints to the beam in the fourth test. The first loading scheme is more realistic in the PT building which responds in the fundamental mode during earthquakes, but the second loading scheme is appropriate in cases where more concentrated response occurs at single floor alone [30].

2.4. Experimental observation

Decompression of the beam-to-column interface and energy dissipation of the system were noticed at an interstory drift of 0.5%. The first test was stopped at an interstory drift of 2% due to bending of the beam flange near the column face (Fig. 6(a)). Longitudinal stresses in the beam flow into the compression toe while the gap opens at the beam-to-column interface, leading to high stress concentrations and web yield at a low drift. The behavior was observed in previous beam–column connection tests [7–9], but bending of the beam flange accompanied by loss of PT forces was never observed. The damage resulted from different details of the flange reinforcing plates adopted in the previous beam–column connection subassemblages and the specimen frame. The flange reinforcing plates were welded outside beam flanges in the prior studies (Fig. 7(a)) but were welded along the edges of beam flanges in the specimen frame (Fig. 7(b)). Although different details had the same cross-sectional area in resisting axial forces at the compression toe, the bending stiffness of reinforced beam flanges was smaller in the frame specimen than in the prior connection specimens. Vertical stiffeners were welded to the beam flange inner side and the beam web to reinforce the compression toe (Fig. 6(b)) so the frame could be retested without further damaging the beam. At an interstory drift of 3%, the RFP in tension forced the jacket plate above or below the beam flange out of the column face, leading to concrete spall (Fig. 6(c)), but no strength degradation was found. Two RFPs, which were attached to the exterior connections, fractured (Fig. 6(d)) when the frame moved towards an interstory drift of 4%. Two fractured RFPs were not replaced for the second test using the same loading protocol and no more RFP fractures occurred during the test.

Fig. 8(a) shows the base shear versus the lateral deformation of column CC in the first two tests; the PT frame apparently dissipated more energy during the first test than during the second test. Six RFPs were removed from the connection after the second test to evaluate the frame response without energy-dissipating devices. The bilinear elastic behavior of the

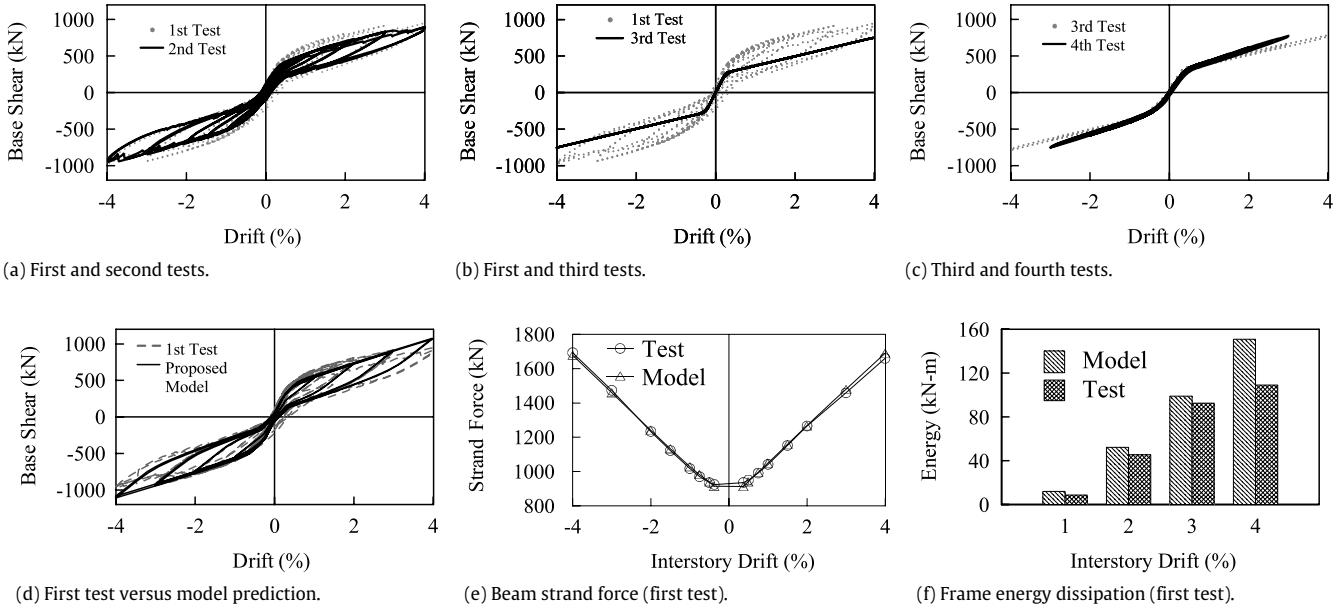

(a) First and second tests. (b) First and third tests. (c) Third and fourth tests.

(d) First test versus model prediction. (e) Beam strand force (first test). (f) Frame energy dissipation (first test).

Fig. 8. Hysteretic responses of the specimen frame.

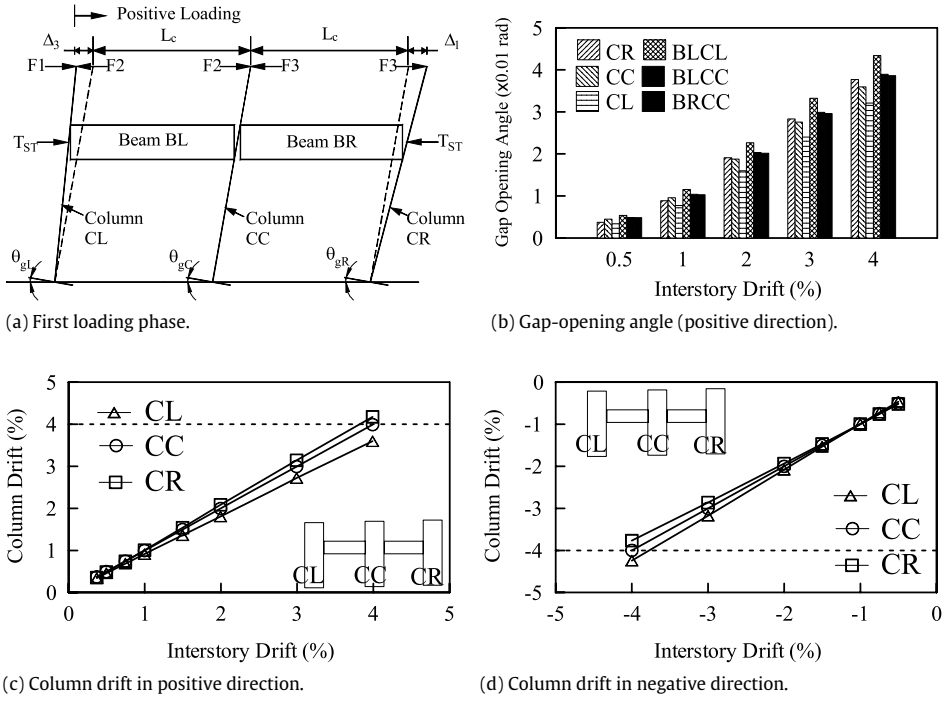

(a) First loading phase. (b) Gap-opening angle (positive direction).

(c) Column drift in positive direction. (d) Column drift in negative direction.

Fig. 9. Column deformation versus drift relationship.

PT frame was observed by comparing the hysteretic loops between the first and third tests (Fig. 8(b)); a 20 mm wide gap-opening between the column face and the beam was observed at a 4% drift (Fig. 6(e)). In the fourth test, the PT frame was loaded with no relative column deformation at the actuator level, leading to zero deformation in Act 3 and Act 4. Conversely, these actuators in the third test expanded due to gap-opening at the beam-to-column interfaces. Because column restraint was greater in the fourth test than in the third test, the post-yielding stiffness of the PT frame was 20% higher in the fourth test than in the third test (Fig. 8(c)). Fig. 6(f) shows minor yielding of the beam web near the termination of the flange reinforcing plate, and buckling of the beam was not observed after the fourth test.

As the gap opens at the beam-to-column interface in a PT frame, the beams push exterior columns outward in order to satisfy deformation compatibility of the frame. Fig. 9(a) shows the schematic deformation of the frame under the first loading case. The beam span in the frame expands from the original length L_c to $L_c + \Delta_1$ and $L_c + \Delta_3$, respectively. Different span lengths result from different locations of the beam compression toe against columns CL and CR. Fig. 9(b) shows gap-openings at the column base and the beam-to-column interface, which were measured by a set of displacement transducers positioned near the interface. Note that under positive bending, the gap-opening angle and the lateral deformation of column CR are larger than those of other columns (Fig. 9(b) and (c)). The gap-opening angle of the beam-to-column interface is larger at the exterior column (BLCL) than at the interior

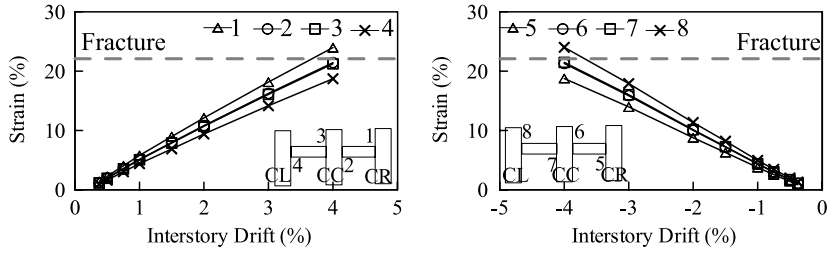

(a) Positive direction. (b) Negative direction.

Fig. 10. Maximum tensile strain of RFP versus drift relationship (first test).

column (BLCC or BRCC). Under negative bending, the gap-opening angle and the lateral deformation of column CR are smaller than those of other columns (Fig. 9(d)).

Fig. 10 shows maximum tensile strains of RFPs in four connections. The strain was computed based on the measured gap-opening, location of the neutral axis, and the axial force–deformation relationship of the RFP. Under positive loading direction (Fig. 10(a)), strain in the RFP of the exterior connection (CR) was largest among all RFPs due to frame expansion; the trend was similar to that of gap-opening angles observed at the column base (Fig. 9(b)). Strain in the RFP of the exterior connection (CR) reached the fracture strain of material at an interstory drift of 4%, leading to fracture of the RFP along the narrowest section (Fig. 6(d)). Under negative loading direction, strain in the RFP of the exterior connection (CL) also reached the fracture strain of material at an interstory drift of −4% (Fig. 10(b)), leading to fracture of the RFP.

3. Analytical modeling of specimen frame

Christopoulos et al. [12] and Chou and Chen [30] demonstrated that the numerical model of the PT connection, using rotational springs in the connection, closely predicts the hysteretic behavior of these types of connections as long as the beam remains elastic. The axial force in the beam during gap-opening can be calculated from the connection moment at the column face. Detailed modeling technique can be found elsewhere [12,30]. This study used the previously suggested scheme with a rotational spring to model the gap-opening, closing behavior at the beam-to-column interface and the column base. The analytical model (Fig. 11) was implemented using the computer program, PISA [32]. Beam–column elements were used to model beams and columns. Three zero-length spring elements connecting nodes of beams and columns were used to model the bilinear elastic behavior of the PT elements (SC Spring), the bilinear elastoplastic behavior of the RFPs (RFP spring), and the column restraint opposing the frame expansion (RE spring). The rotational spring model greatly reduces the number of nodes in the beam–column connection compared to the traditional fiber model or axial spring model. The cyclic response of the specimen frame and the strand force in the beam modeled based on the rotational spring scheme were close to those in the first test (Fig. 8(d) and (e)). Note that the base shear was overestimated after a 3% drift due to RFP fractures, which were not considered in the model. The area within the hysteresis loops was integrated up to an interstory drift of 4% to determine *Eh*, which is the accumulated energy dissipation. The analytical model has energy dissipation similar to the specimen frame before two RFPs fracture at an interstory drift of 4% (Fig. 8(f)).

Fig. 12(a) shows the base shear versus lateral deformation of the analytical model and the specimen frame in the third and fourth tests; no energy dissipation was obtained because no RFPs were considered in the model. Although the RE spring at the base simulated the column restraint to the frame expansion, gap-opening angles were the same at the base of all columns and PT force variation in columns was symmetric in both loading directions (Fig. 12(b)). The maximum error in PT force prediction was about 16% in the fourth test. Since the frame in the third test expanded easily due to minor column restraints, the axial force in the beam was similar to the applied strand force (Fig. 12(c)). Moreover, the PT frame in the fourth test was loaded with no relative column deformation at actuator level, column restraints resulted in larger axial force in the beam than in the strands (Fig. 12(d)). Different axial loads in the beams and the strands can also be obtained by the computer model using the rotational spring scheme. By comparing results obtained from the model to experimental results, it is confirmed that this rotational spring model approach, as shown in Fig. 11, captures well the cyclic responses of the specimen frame. However, different gap-opening angles at the base of PT columns cannot be predicted.

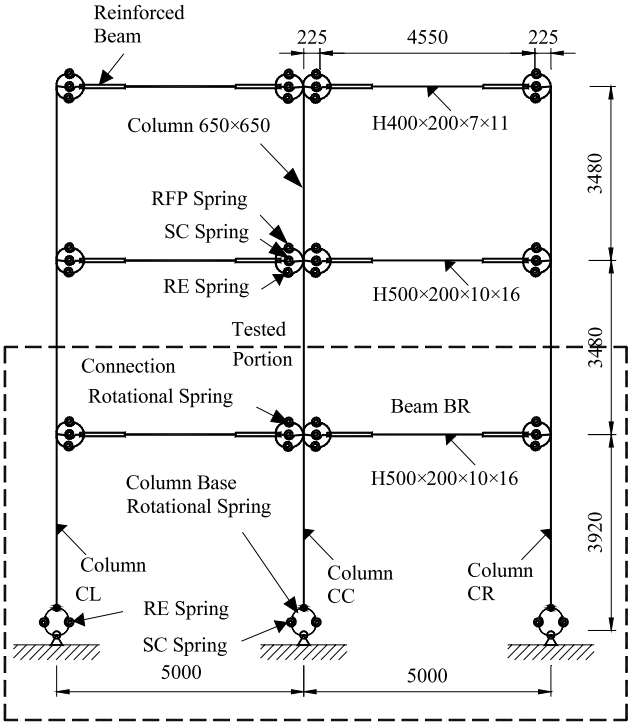

Fig. 11. Specimen model and three-story frame model.

4. Seismic response of a post-tensioned frame

Nonlinear time-history analyses were performed on the three-story prototype building using the PISA computer program. Axial forces due to gravity loads were assigned at each column node. Fixed end moments and shear forces caused by gravity loads on

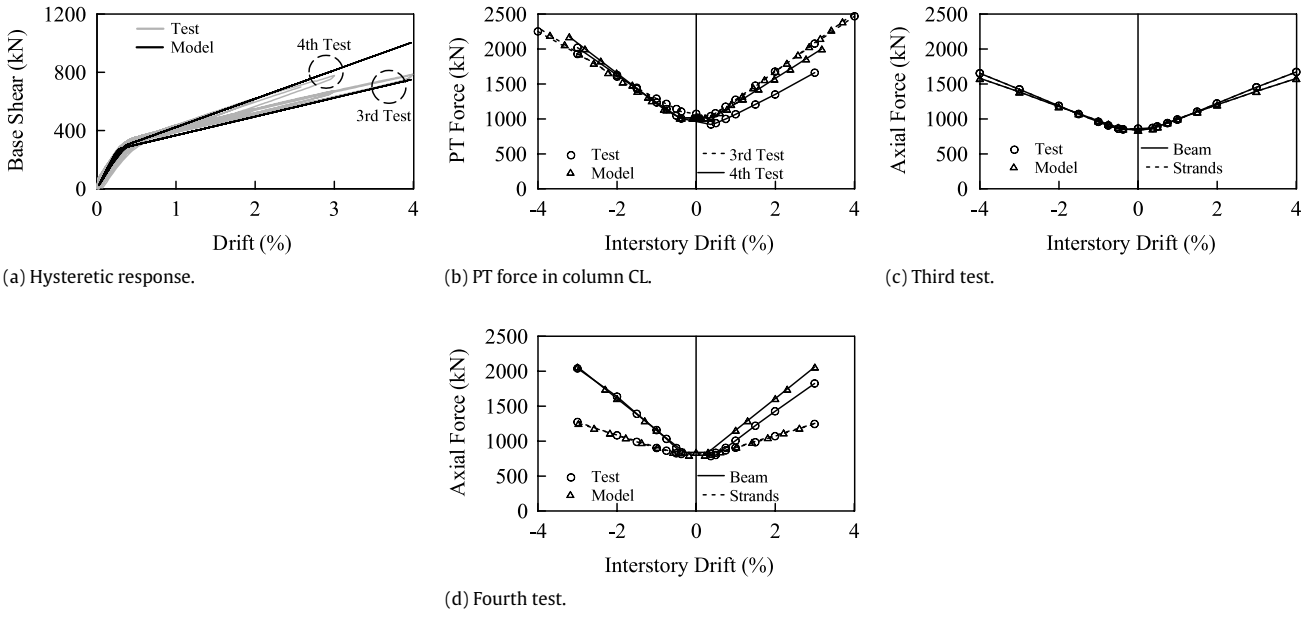

(a) Hysteretic response.

(b) PT force in column CL.

(c) Third test.

(d) Fourth test.

Fig. 12. Comparison between frame test results and analytical model prediction.

Table 2
Ground motion data.

Earthquake	Record	PGA (g)	Scale factor	Scaled PGA	Site conditions	Distance (km)	Station
Superstition hills	WSM180	0.21	1.83	0.38	D	13	11,369 Westmoreland fire station
	ICC090	0.25	1.83	0.46	D	14	01,335 El Centro Imp. Co. Cent
Chi–Chi	TCU074	0.60	0.64	0.38	D	18	–
	TCU039	0.21	1.94	0.40	D	17	–
	TCU034	0.25	1.45	0.36	C	33	–
Loma Prieta	CAP090	0.38	1.30	0.49	D	15	47,125 Capitola
	AND360	0.24	2.08	0.50	C	21	1652 Anderson Dam (Downstream)
	STG090	0.32	1.76	0.57	C	13	58,065 Saratoga-Aloha Ave
Landers	IND090	0.11	3.60	0.39	D	56	12,026 Indio-Coachella canal
	PSA090	0.09	3.91	0.35	D	38	12,025 Palm springs airport
	JOSHUA90	0.28	1.48	0.41	C	11	22,170 Joshua tree
Northridge	LOS270	0.48	0.90	0.43	D	13	90,057 Canyon country-W lost cany
	CNP196	0.42	1.13	0.47	D	16	90,053 Canoga park-topanga can
	MUL279	0.52	0.57	0.29	C	20	90,013 Beverly hills-14145 mulhol
	CAST360	0.51	0.78	0.40	C	21	24,278 Castaic-old ridge route

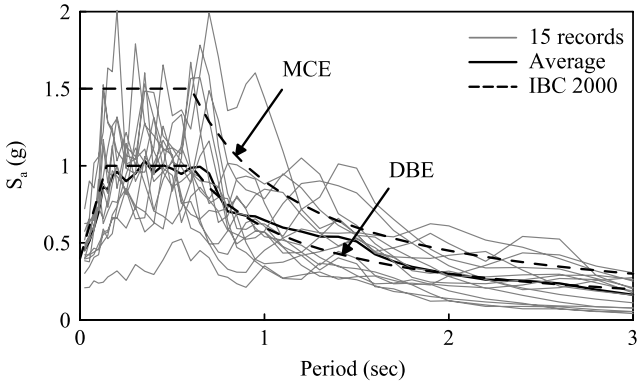

Fig. 13. Response spectra.

the beams were applied at the ends of the elements representing the beam members. A Rayleigh type damping of 5% of critical was assigned in the first mode and the third mode. The rotational spring element was used at each connection and column base as the specimen frame to simulate the self-centering hysteretic behavior. Since the frame adopted the slab, which is restrained to PT beams along the frame direction but allows for the gap-openings to be accommodated along the column lines [9,17,18], floor masses were equally assigned to all nodes in the same floor for dynamic analyses. The panel zone deformation and the P–Delta effects due to gravity loading were not considered in the model.

An ensemble of 15 strong ground motions was chosen from earthquake records that were recorded in California or in Taiwan. These records were free of any forward directivity effects (near-field effects) and were recorded for soil types C or D, generated by earthquakes of moment magnitude ranging from 6.7 to 7.3. A 5% damped design earthquake response spectrum for buildings built on soil class D was constructed and was used as the target spectrum [27]. Each record was scaled to minimize the square of error between its 5% damped response spectrum and the target spectrum, which represents the design spectrum for DBE level. Table 2 lists ground motion data for each record and Fig. 13 presents response spectra for each of the 15 scaled records along with the target spectrum. A good match exists between mean spectra values and the target spectrum although small deviations can be observed in the medium period ranges (periods between 1 and 1.7 s), which are beyond the fundamental period of the frame (0.7 s). In addition, the DBE ground motions were scaled by a factor

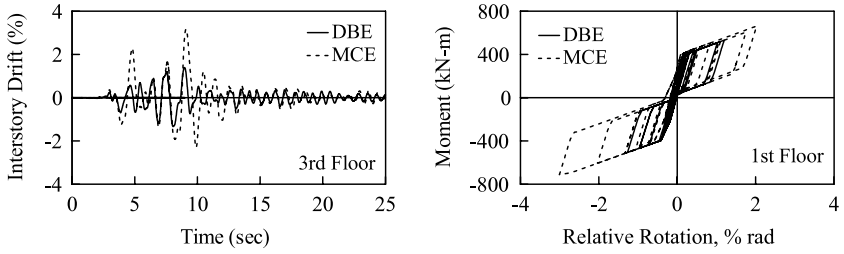

(a) Northridge-CNP196.

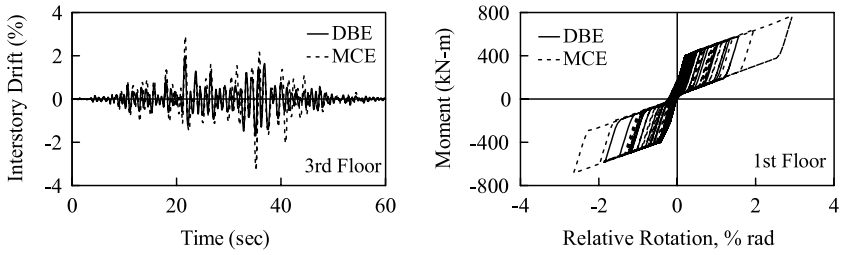

(b) Lander-PSA090.

Fig. 14. Displacement responses and connection hysteresis loops.

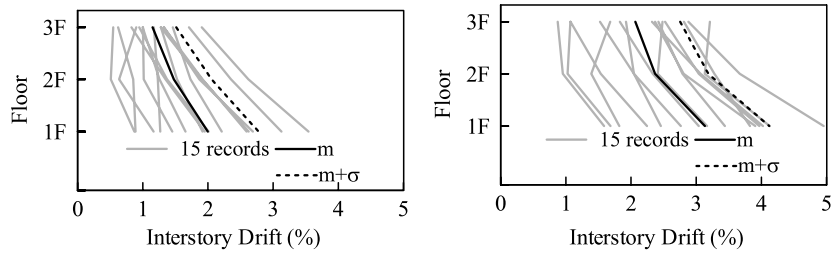

(a) DBE level. (b) MCE level.

Fig. 15. Maximum floor displacement profiles.

of 1.5 to investigate the seismic demands of the proposed frame under MCE level ground motions.

Time-history analyses of the PT frame under the 1994 Northridge and 1992 Lander ground motions were first presented to illustrate the seismic responses. The maximum interstory drifts of the frame subjected to DBE and MCE level earthquakes were lower than 2% and 4% (Fig. 14). From the moment–rotation relationship of the connection, it was also found that the decompression of the beam-to-column interface starts at about 0.5% and the flag-shaped hysteretic response can be maintained with increasing displacement amplitudes.

Fig. 15 presents the distribution along the building height of the mean (m) and mean plus one standard deviation ($m + \sigma$) values of the seismic response indices. The maximum interstory drift demands of the second and third floors are lower than those of the first floor for most cases. Although the mean values of maximum drift of the PT frame under DBE and MCE level earthquakes are about 2% and 3%, which are within the self-centering limit 4% during the test, the maximum ($m + \sigma$) value of interstory drift of the PT frame under MCE level earthquakes is 4.1% on the first floor, which is close to the limit. Furthermore, all floors in the PT frame experiences almost constant residual drift less than 0.1% for both the mean and $m + \sigma$ values (Fig. 16).

5. Conclusions

A three-story prototype building was designed as a post-tensioned self-centering moment frame according to the design procedure [14] with modification by taking into account the frame expansion [30]. A full-scale one-story two-bay specimen frame, which was a substructure of the prototype PT building using reinforced concrete columns and steel beams, was tested in the Taiwan National Center for Research on Earthquake Engineering. The objectives of the tests were aimed at presenting (1) data about connection performance, progress of damage, and strength degradation of the frame, and (2) comparison between the experimental and analytical results of the specimen frame in terms of the cyclic response, energy dissipation, and PT force variation. Inelastic time-history analyses were also conducted to examine the seismic responses of the prototype frame subjected to DBE and MCE level earthquakes. Based on these tests and analyses, summaries and conclusions are made as follows:

1. Bending of the beam end in the specimen frame was never observed in prior tests of beam–column subassemblages, which had flange reinforcing plates welded outside beam flanges. By comparing details of the flange reinforcing plates from the connection specimen to the frame specimen, it was found that welding flange reinforcing plates along the edges of beam flanges in the frame specimen decreased the bending stiffness of reinforced beam flanges and resulted in the damage of beam flanges, accompanied by loss of PT forces. Therefore, it was not a good idea to reinforce the beam by extending the beam flange from the edges.
2. Tests confirmed that energy dissipation of the specimen frame was provided by the RFPs of all connections and the beam could remain elastic up to a 4% drift. Deformation demands imposed on RFPs of the exterior connections were larger than those of the interior connection due to frame expansion, leading to fractures of RFPs in the exterior connections.

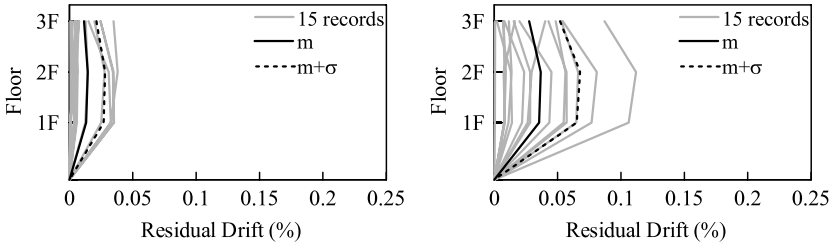

(a) DBE level. (b) MCE level.

Fig. 16. Residual floor drift profiles.

3. The hysteretic response and energy dissipation of the specimen frame could be satisfactorily simulated by a computer model using the rotational spring scheme. However, the error in predicting the PT forces in columns ranged from 5% to 16% due to different gap-opening angles at the base of exterior and interior columns.
4. The mean values of maximum interstory drift of the PT frame under DBE and MCE level earthquakes are about 2% and 3%; the maximum $(m + \sigma)$ value of an interstory drift of the PT frame under MCE level earthquakes is about 4% on the first floor, close to the fracture limit state of the RFPs in the specimen frame.

Note that the effect of the separated slab system on gap-openings at beam-to-column interfaces is minimal based on the prior studies [9,17,18], so the slab was not incorporated in the specimen. Loading from the column instead of the slab to the specimen was adopted to study the frame response and column restraints to the frame expansion. Although this method of loading did not represent what would actually occur in a real building, the damage of the beam was discovered from the static test. The effect of the compression force in the beam due to the lateral inertia force needs to be further investigated.

Acknowledgements

The test program was supported by the National Center of Research on Earthquake Engineering (NCREE), Taiwan with Prof. K.C. Tsai as the program director. The writers are grateful to Prof. H.L. Hsu of National Central University and Dr. K.C. Lin of NCREE for their corporation on the design and construction of the specimen frame.

References

[1] Sakaguchi N, Tominaga H, Murai Y, Takase Y, Shuto K. Strength and ductility of steel beam-RC column connection. In: Proc. 9th world conf. on earthquake eng., IV. Tokyo-Kyoto (Japan): 1988. pp. 713–8.
[2] Griffis LG. Composite frame construction. In: Dowling PJ, et al., editors. Constructional steel design. Elsevier Science Publishers; 1992. p. 523–53.
[3] Kanno R, Deierlein G. Seismic behavior of composite (RCS) beam–column joint subassemblies. Composite Construction 1996;III:1–14.
[4] Chou CC, Uang CM. Cyclic performance of a type of steel beam to steel-encased reinforced concrete column moment connections. Journal of Constructional Steel Research 2002;58:637–63.
[5] Chou CC, Uang CM. Effects of continuity plate and transverse reinforcement on cyclic behavior of SRC moment connections. Journal of Structural Engineering, ASCE 2007;133(1):96–104.
[6] Chou CC, Wu CC. Performance evaluation of steel reduced flange plate moment connections. Earthquake Engineering and Structural Dynamics 2007;36(14):2083–97.
[7] Chou CC, Chen JH, Chen YC, Tsai KC. Evaluating performance of post-tensioned steel connections with strands and reduced flange plates. Earthquake Engineering and Structural Dynamics 2006;35(9):1167–85.
[8] Chou CC, Lai YJ. Post-tensioned self-centering moment connections with beam bottom flange energy dissipators. Journal of Constructional Steel Research 2009;65(10):1931–41.
[9] Chou CC, Weng CY, Chen JH. Seismic design and behavior of post-tensioned connections including effects of a composite slab. Engineering Structures 2008;30:3014–23.
[10] Ricles JM, Sause R, Garlock M, Zhao C. Posttensioned seismic-resistant connections for steel frames. Journal of Structural Engineering, ASCE 2001;127(2):113–21.
[11] Ricles JM, Sause R, Peng SW, Lu LW. Experimental evaluation of earthquake resistant posttensioned steel connections. Journal of Structural Engineering, ASCE 2002;128(7):850–9.
[12] Christopoulos C, Filiatrault A, Uang CM, Folz B. Posttensioned energy dissipating connections for moment-resisting steel frames. Journal of Structural Engineering, ASCE 2002;128(9):1111–20.
[13] Chou CC, Tsai KC, Chen JH, Chen YC, Chuang SC. Cyclic behavior of post-tensioned steel connections with reduced flange plate and slab. In: 1st international conference on advances in experimental structural engineering, 2005.
[14] Garlock MM. Full-scale testing, seismic analysis, and design of post-tensioned seismic resistant connections for steel frames. Ph.D. dissertation. Civil and Environmental Engineering Dept. Bethlehem (PA): Lehigh Univ.; 2002.
[15] Garlock MM, Ricles JM, Sause R. Experimental studies of full-scale posttensioned steel connections. Journal of Structural Engineering, ASCE 2005;131(3):438–48.
[16] Garlock MM, Liu J, King A. Construction details for self-centering moment resisting frame floor diaphragms. In: US Taiwan workshop on self-centering structural systems. 2006.
[17] Kim HJ, Christopoulos C. Seismic design procedure and seismic response of post-tensioned self-centering steel frames. Earthquake Engineering and Structural Dynamics 2008;38(3):355–76.
[18] Chou CC, Tsai KC, Yang WC. Self-centering steel connections with steel bars and a discontinuous composite slab. Earthquake Engineering and Structural Dynamics 2009;38(4):403–22.
[19] Priestley MJN. Overview of the PRESSS research program. PCI Journal 1991;36:50–7.
[20] Pampanin S, Priestley MJN, Sritharan S. PRESSS Phase 3: the five-story precast test building-frame direction response. Report No. SSRP 2000/08. La Jolla (CA): University of California San Diego; 2000.
[21] Christopoulos C, Filiatrault A, Uang CM. Shake table testing of a steel moment frame assembly with post-tensioned energy dissipating connections. In: Proceedings of 7th US national conference on earthquake engineering. 2002.
[22] Lin YC, Ricles JM, Sause R. Earthquake simulations on a self-centering steel moment resisting frame with web friction devices. In: 14th world conference on earthquake engineering. 2008.
[23] Tsai KC, Chou CC, Lin CL, Chen PC, Jhang SJ. Seismic self-centering steel beam-to-column moment connections using bolted friction devices. Earthquake Engineering and Structural Dynamics 2008;37:627–45.
[24] Wang D, Filiatrault A. Shake table testing of a self-centering post-tensioned steel frame. In: 14th world conference on earthquake engineering. 2008.
[25] Chou CC, Chen YC. Cyclic tests of post-tensioned precast CFT segmental bridge columns with unbonded strands. Earthquake Engineering and Structural Dynamics 2006;35:159–75.
[26] Chou CC, Hsu CP. Hysteretic model development and seismic response of unbonded post-tensioned precast CFT segmental bridge columns. Earthquake Engineering and Structural Dynamics 2008;37:919–34.
[27] IBC. International Building Code. International Code Council, Falls Church. Virginia: 2000.
[28] Rojas P. Seismic analysis, design, and evaluation of post-tensioned friction damped connections for steel moment resisting frames. Ph.D. dissertation. Civil and Environmental Engineering Dept. Bethlehem (PA): Lehigh Univ.; 2003.
[29] American Concrete Institute (ACI) 318. Building code requirements for structural concrete (ACI 318M-02) and commentary (ACI 318RM-02). Farmington Hills (MI): American Concrete Institute; 2002.
[30] Chou CC, Chen JH. Column restraint in post-tensioned self-centering moment frames. Earthquake Engineering and Structural Dynamics 2009; Available online 2009/11.
[31] AISC. Seismic provisions for structural steel buildings. Chicago (IL): AISC; 2005.
[32] Tsai K-C, Lin B-Z. Development of an object-oriented nonlinear static and dynamic 3D structural analysis program. CEER/R92-04. Center for Earthquake Engineering Research, National Taiwan University; 2003.